We are IntechOpen, the world's leading publisher of Open Access books Built by scientists, for scientists

6,900
Open access books available

185,000
International authors and editors

200M
Downloads

Our authors are among the

154
Countries delivered to

TOP 1%
most cited scientists

12.2%
Contributors from top 500 universities



WEB OF SCIENCE™

Selection of our books indexed in the Book Citation Index in Web of Science™ Core Collection (BKCI)

Interested in publishing with us?
Contact book.department@intechopen.com

Numbers displayed above are based on latest data collected.
For more information visit www.intechopen.com



Chapter 19

New Photo-Thermo-Refractive Glasses for Holographic Optical Elements: Properties and Applications

Nikonorov Nikolay, Ivanov Sergey,
Dubrovin Victor and Ignatiev Alexander

Additional information is available at the end of the chapter

http://dx.doi.org/10.5772/66116

Abstract

This chapter presents a survey of recent achievements of the ITMO University (St. Petersburg, Russia) in developing new holographic media such as fluoride, chloride, and bromide silicate photo-thermo-refractive (PTR) glasses as well as the holographic diffractive optical elements that are the volume Bragg gratings recorded in the glasses for improving dramatically the parameters of laser systems of different types. The photo-thermo-induced crystallization process and the properties of fluoride, chloride, and bromide PTR glasses are demonstrated. This new technology enabled recording high-efficiency phase volume holograms in the optical quality silicate glass. These holograms are used for developing a number of unique diffractive optical elements that provide new opportunities for the laser technique. Some examples of designing and fabricating of holographic optical elements such as the super-narrowband filters for solid-state lasers and laser diodes, laser beam combiners, and collimator sights are demonstrated in this chapter. It is shown that the PTR glass doped with rare earth ions can be used for designing lasers with Bragg reflectors and distributed feedback.

Keywords: PTR glass, photo-thermo-refractive glass, photo-thermo-induced crystallization, volume Bragg grating, beam combining, refractive index, photosensitive glass

1. Introduction

Photo-thermo-refractive (PTR) glasses are a new class of photosensitive materials intended for recording three-dimensional (3D) phase holograms. This class was developed based on photo-sensitive sodium zinc aluminosilicate glasses that were first put into practice by

INTECH
open science | open minds

© 2017 The Author(s). Licensee InTech. This chapter is distributed under the terms of the Creative Commons Attribution License (http://creativecommons.org/licenses/by/3.0), which permits unrestricted use, distribution, and reproduction in any medium, provided the original work is properly cited. CC BY

Corning, Inc., in 1977 and were referred to as polychromatic (PC) glasses [1–3]. In Russia, similar photosensitive glasses [4, 5] were denoted by multichromatic (MC) ones. PC/MC glasses are known to contain, in addition to Na_2O, Al_2O_3, ZnO, and SiO_2, some other ingredients such as (i) photosensitive dopants playing the roles of electron donors (Ce^{3+}) and acceptors (Ag^+, Sb^{5+}, and Sn^{4+}) and also (ii) halogen ions (F^- and Br^-) that participate in the formation of the crystalline phases. The main specific feature of PC/MC glasses is the selective absorption in the visible. Namely, PC glasses can acquire, under the effects of the UV exposure and subsequent heat treatment, a wide variety of colors. In brief, the final stages of photochemical and diffusion processes responsible for this coloration were assumed to be as follows. The colloidal silver particles formed under the above effects play the role of nucleation centers. Around such centers, the growth of NaF and (Ag, Na)Br nano- or microcrystals occurs. Under particular growth conditions, the microcrystals acquire complicated anisotropic shapes such as the elongated pyramid-like structures stretched along an axis [1, 3, 6]. Additional multistage UV irradiation and heat treatment lead to the photolytic precipitation of silver layer on the surfaces of these anisotropic structures (so-called "decoration of the latter with silver"). The anisotropy of metallic silver shells thus formed results in a certain shift of the corresponding absorption band into the visible. So the substantial anisotropy of metallic silver particles was considered to be the principal condition for the occurrence of "PC/MC coloration" in PC/MC glasses.

In the late 1980s–early 1990s [7–10], it was proposed first in Vavilov State Optical Institute to apply PC/MC glasses for recording the 3D phase holograms. Unlike the case of PC/MC coloration, only a single stage of photo-thermo-induced crystallization was used, and this stage included the UV irradiation and subsequent heat treatment. When developing the corresponding procedures, the principal attention was paid to a difference obtainable in the refractive indices of vitreous and crystalline phases rather than the anisotropic shapes of microcrystals. As a result, a new class of materials was developed in Vavilov State Optical Institute, this class was denoted [10] by a specific term such as "photo-thermo-refractive (PTR) glasses" (i.e., glasses whose refractive index varies due to the UV irradiation and subsequent heat treatment). Later [11, 12], this term started to be used widely in other countries as well. Now, there is an increased interest in PTR glasses because the volume Bragg gratings recorded on these glasses reveal a unique combination of working characteristics such as the high angle and spectral selectivity, high diffraction efficiency, high mechanical and optical strength, and also high thermal and chemical durability. Based on PTR glasses, a broad variety of optical devices are developed including extra narrow-band filters, wavelength division multiplexing (WDM) devices, combiners of high-intensity light beams, chirped gratings for compressing the light impulses, filters for increasing the spectral brightness of laser diodes, etc.

The given paper is a survey of recent achievements of ITMO University (St. Petersburg, Russia) in developing new holographic media such as fluoride, chloride, and bromide silicate photo-thermo-refractive (PTR) glasses as well as the holographic diffractive optical elements that are the volume Bragg gratings recorded in the glasses for improving dramatically the parameters of laser systems of different types.

http://dx.doi.org/10.5772/66116

2. Properties of fluoride PTR glasses

The fluoride PTR glass was designed and synthesized in ITMO University, Russia [12]. The fluoride PTR glass is a photosensitive multicomponent sodium-zinc-alumino-silicate one containing fluorine (6 mol%) and small amount of bromine (0.5 mol%) and also doped with additives (cerium, antimony, and silver) that are responsible for the photo-thermo-induced precipitation of silver nanoparticles and sodium fluoride crystals—see for example [1, 13, 14]. Untreated fluoride PTR glasses are transparent in a wide spectral range of 250–2500 nm (**Figure 1(a)**). The selective UV irradiation into the Ce^{3+} absorption band in the spectra of these glasses results in the formation of neutral silver molecular clusters. The subsequent heat treatment of UV-irradiated PTR glasses near the glass transition temperature (T_g) induces the silver nanoparticle formation [1] (**Figure 1(b)**). The thermal treatment of these glasses at temperatures above T_g leads to the growth of silver bromide shell on a silver nanoparticle [15] and then to the precipitation of sodium fluoride cone on it [1, 16]. Image of XRD pattern of UV-exposed and thermal-treated PTR glass sample is shown in **Figure 2**.

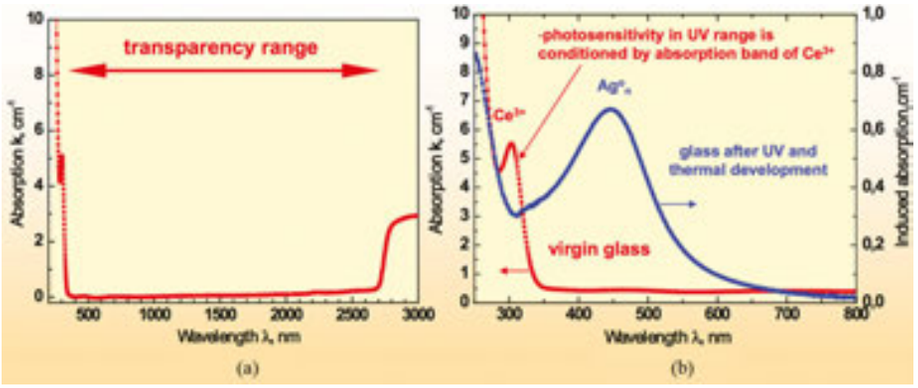


Figure 1. Absorption spectra of (a) virgin PTR glass and (b) the glass sample after the UV irradiation and subsequent heat treatment.

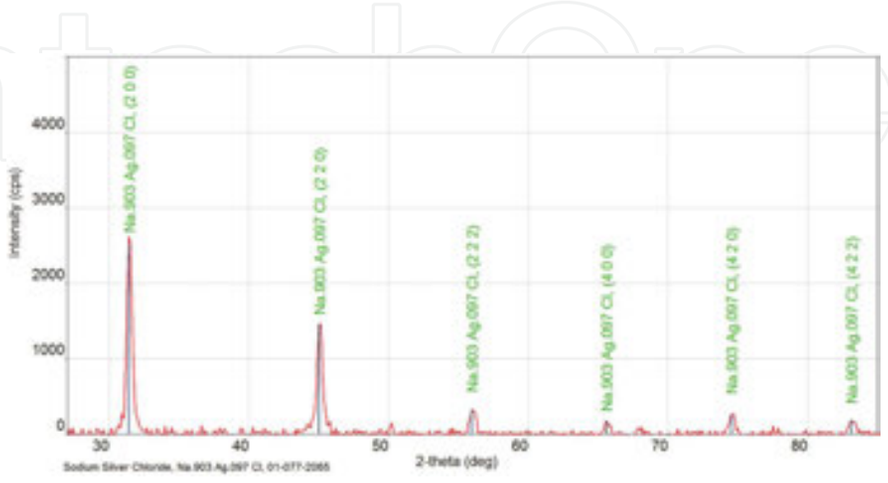


Figure 2. X-ray diffraction pattern of UV-irradiated and thermal-treated PTR glass.

In Ref. [13], authors showed, for the first time, the dramatic effect of bromine on the process of NaF crystal growth in fluoride PTR glasses. The paper has demonstrated that the growth of sodium fluoride crystals is possible only in the presence of bromide additives in the PTR glass composition. A generalized NaF crystallization mechanism that consists of three stages is proposed in Refs. [1, 17].

The process of photo-thermo-induced crystallization of fluoride PTR glass is shown schematically in **Figure 3**.

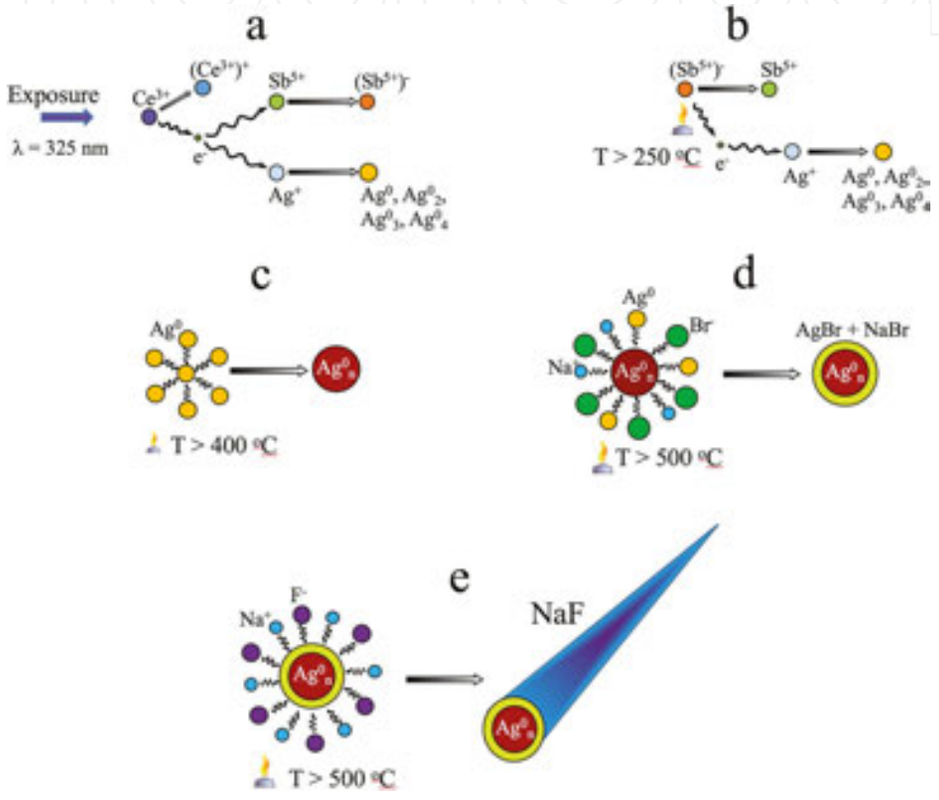


Figure 3. Photo-thermo-induced crystallization of fluoride PTR glass. (a) Cerium photoionization and trapping the photoelectrons by Sb; (b) Releasing electrons Sb and trapping them by Ag ions with the formation of neutral silver atoms and clusters; (c) Formation of colloidal particles under heating up to 400°C; (d) Growth of (Ag, Na)Br shell on colloidal silver particles at $T > 500$°C; (e) Growth of NaF microcrystals at $T > 500$°C.

At the first stage, the trivalent cerium ion donates an electron under the effect of the UV irradiation, thus increasing its own valency in accordance with the following reaction (**Figure 3(a)**)

$$Ce^{3+} + h\nu \rightarrow e^{-} + \left[Ce^{3+}\right]^{+} \tag{1}$$

Released photoelectrons can be trapped partially by silver ions (~20%) with subsequent neutral silver atom and molecular cluster formation (Ag^0, Ag_2^0, Ag_2^+, Ag_3^{2+}), but most photoelectrons are trapped by antimony ions according to the following reaction (**Figure 3(b)**):

$$e^- + Sb^{5+} \rightarrow \left[Sb^{5+}\right]^- \quad (2)$$

At the second stage, the heat treatment at relatively low temperatures (300–450°C) leads to releasing the trapped electrons from antimony (**Figure 3(c)**) with further formation of silver molecular clusters and colloidal nanoparticles (**Figure 2(b)**):

$$\left[Sb^{5+}\right]^- \rightarrow Sb^{5+} + e^- \quad (3)$$

$$nAg^+ + ne^- \rightarrow nAg^0 \quad (4)$$

At the third stage, the heat treatment at temperatures above T_g results, first, in the growth of mixed silver bromide-sodium bromide shell on a silver nanoparticle (**Figure 3(e)**) and, further, in the coaxial growth of sodium fluoride crystalline phase on this shell (**Figure 3(g)**).

In Ref. [15], authors showed that the UV irradiation and subsequent heat treatment of fluoride PTR glass induces the refractive index change only in the UV-irradiated area. There is still some uncertainty in the origin of refractive index change in PTR glass, and several presumable mechanisms of the change are discussed. Classically, this effect is assumed to be caused by difference in the refractive indices between the NaF crystal phase (n ~ 1.33) sedimented in the UV-irradiated area and the unexposed glass area (n ~ 1.49) so that the precipitation of sodium fluoride leads to the negative refractive index increment. Although a difference between the refractive indices of sodium fluoride and vitreous phase is rather big, the negative refractive index change in the UV-irradiated area does not exceed 1×10^{-3} [15, 18]. This can probably be due to the fact that, in addition to the NaF phase precipitation, there is also the silver bromide shell with a high refractive index value (n ~ 2.3) on the silver nanoparticle. As shown in many sources (see for example Refs. [14, 19, 20]), the maximum of surface plasmon resonance of silver nanoparticles in fluoride PTR glasses shifts to the greater wavelengths owing to the silver bromide shell growth.

On the other hand, the authors of [21] proposed another possible mechanism of photo-thermo-induced refractive index change in PTR glass. They assumed that the transformation of Na^+ and F^- distributed in the PTR glass matrix into the crystalline NaF (a chemical change) and structural relaxation process are not the main causes of photo-thermo-induced refractive index change and assigned this change to high residual stresses around the NaF crystals. According to calculations presented in the paper, these stresses are the most important cause for the photo-thermo-induced refractive index change in PTR glass.

Also, fluoride PTR glasses have outstanding mechanical, optical, and chemical properties. In particular, they show a high photosensitivity, high thermal stability of the recorded phase holograms, and high tolerance to the optical and ionizing irradiation. The basic optical and spectral properties of PTR glass are described in Refs. [14, 22–24]. The holographic optical elements (HOE)s recorded on the PTR glass demonstrate high chemical stability, thermal,

mechanical and optical strength and also reveal, from this point of view, practically no difference with the commercial optical glass BK7 (Schott). The optical and spectral parameters of the HOEs and gradient index (GRIN)-elements do not change after its multiple heating to high enough temperature (500°C). The important advantages of PTR glass as the optical medium are as follows:

i. High optical homogeneity (the refraction index fluctuations across the glass bulk are of the order of 10^{-5}).

ii. Reproducibility of its parameters from one glass synthesis to another and also in the course of the photo-thermo-induced crystallization.

iii. PTR glass can be subjected, similar to optical glass BK7, to various kinds of both the mechanical processing such as grinding and polishing and the formation technologies such as molding, aspheric surface production, and drawing fiber.

iv. One can fabricate PTR glass both in the laboratory conditions (hundreds of grams) and industrial ones (hundreds of kilograms) using a simple and nontoxic technology. The chemical reagents required for the glass fabrication are commercially available and not too expensive.

Transparency range, nm	350–3000
Photosensitivity spectral range, nm	280–350
Photosensitivity, mJ/cm^2	50
RI change, Δn, ppm	1000
RI modulation amplitude, δn, ppm	500
Induced optical loss, cm^{-1}	
• visible range	0.1
• near IR range	0.01
Optical resistance (laser-induced damage threshold):	
• CW regime, kW/cm^2	10
• Nanosecond pulse regime, J/cm^2	40 (Data of University of Central Florida)
Mechanical and thermal resistance, chemical durability	Close to commercial optical glass BK7
Spatial frequency VBGs, mm^{-1}	up to 10,000 (Data of University of Central Florida)
Diffraction efficiency, %	95
Hologram thickness, mm	0.1–10
Angular selectivity, ang. min	<1
Bandwidth FWHM, nm	0.1
Size, mm	up to 25 × 25
VBGs are completely stable at temperature, °C	500
VBGs are completely stable at temperature, °C	500

Table 1. Characteristics of PTR glass and VBGs recorded on the glass.

http://dx.doi.org/10.5772/66116

One should also note some features of PTR glass that are unusual for other recording media. For example, PTR glass can be processed with the ion exchange technology, which provides possibilities (i) to fabricate the ion-exchanged optical [25] or plasmonic waveguides and (ii) to implement the surface strengthening, thus improving the mechanical strength, chemical stability, and thermal and also optical strength.

Some characteristics and advantages of fluoride PTR glasses and also of holographic volume Bragg gratings (VBG) recorded on the glasses are presented in **Table 1** [26].

3. Properties of chloride PTR glasses

The chloride PTR glasses are photosensitive multicomponent glasses based on Na_2O-ZnO-Al_2O_3-SiO_2-NaF system doped with variable batch concentration of Cl (0–2.2 mol%), a photosensitizer such as CeO_2 (0.01 mol%), a reducer such as Sb_2O_3 (0.05 mol%), and also Ag_2O (0.15 mol%). The chloride PTR glass was designed and synthesized in ITMO University, Russia [24].

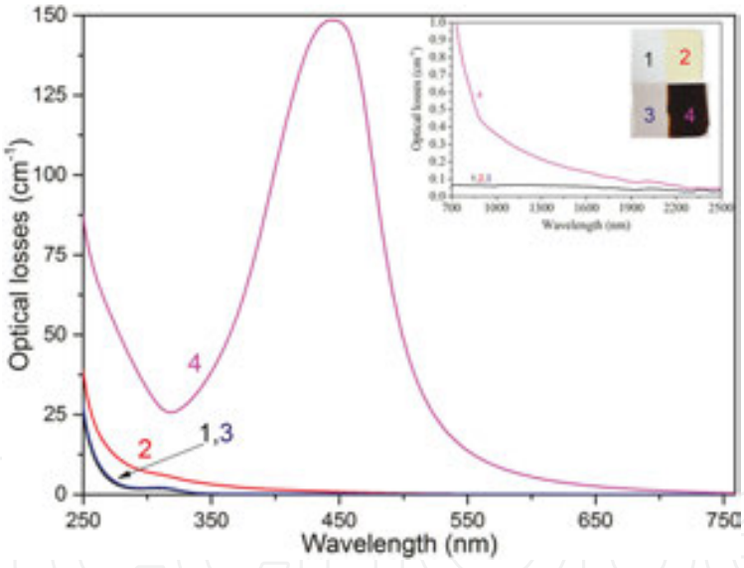


Figure 4. The evolution of the absorption spectra of PTR glass containing 2.2 mol% Cl during photo-thermo induced cristallization (1) is the spectrum for initial untreated glass, (2) is that for glass after the UV irradiation for 50 s alone, (3) is the spectrum for glass after the heat treatment alone at 550°C for 3 h, and (4) is the spectrum for glass after the UV irradiation for 50 s and subsequent heat treatment at 550 °C for 3 h. An inset shows the photos and absorption spectra (700–2500 nm) of treated chloride PTR glass samples containing 2.2 mol% Cl. Here (1) is initial untreated glass, (2) is glass after the UV irradiation for 50 s alone, (3) is glass after the heat treatment alone, and (4) is glass after the UV irradiation for 50 s and subsequent heat treatment.

With changing the type of halide (fluoride to bromide or chloride) in the PTR glass composition, it is possible to control the sign of the RI increment. As mentioned above, for the case of fluoride PTR glass, thermal treatment at temperatures higher than T_g results in a decrease in the RI of the UV-irradiated area in comparison with that of nonirradiated area. On the other

hand, the substitution of fluorine by chlorine leads to the precipitation of nano-crystalline phases of mixed silver and sodium chlorides in glass host and to the positive increment of RI (Δn up to 1.0×10^{-3}) [24].

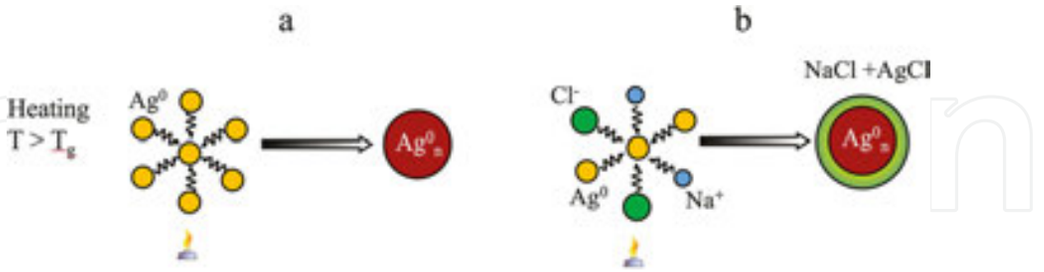


Figure 5. Scheme for the photo-thermo-induced crystallization mechanism inherent in chloride PTR glasses for various Cl concentrations (0–2.2 mol%). (a) Is the growth of shell-free silver nanoparticles in glasses containing 0–1.0 mol% Cl. (b) Is the growth silver nanoparticles with a shell composed of mixed silver and sodium chlorides in glasses containing 0–2.2 mol% Cl.

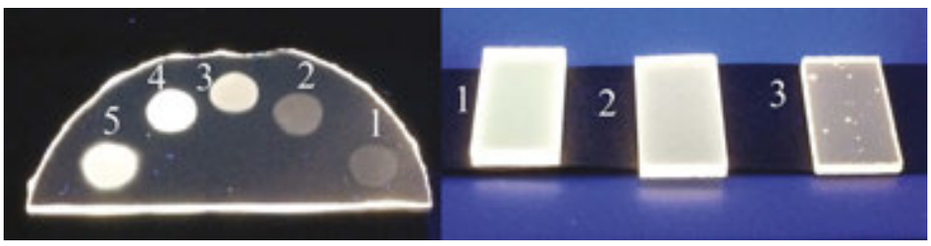


Figure 6. Photos of chloride PTR glass luminesce under UV (λ = 365 nm) excitation (a) is the photo of PTR glass containing 1 mol% Cl after the UV irradiation with various doses. The exposure duration (sec) that sets a dose is (1) 0.5 s, (2) 1 s, (3) 5 s, (4) 50s, (5) 500 s; (b) is the photo of the UV-irradiated and heat treated (1 h 400°C) chloride PTR glasses differing in the chlorine concentration. The chlorine concentrations (mol%) being (1) 0, (2) 1, and (3) 2.

Initially, chloride PTR glasses are transparent in a wide spectral range. 250–2500 nm (**Figure 4**). The UV irradiation of chloride PTR glasses results in the Ce^{3+} ion photoionization and the resultant formation of silver molecular clusters (SMC), the latter playing the role of crystallization centers (**Figures 4** and **5**). Heating all studied chloride PTR glasses at temperatures above 250°C and less than T_g results, as shown in **Figure 5(b)**, in releasing electrons from Sb and capturing them by Ag ions with further formation of an extra amount of neutral silver atoms and molecular clusters [19]. The latter provide, according to Refs. [27, 28], a broadband luminescence in the visible and NIR ranges (**Figure 6**). Further, the heat treatment of PTR glasses containing 0–1.0 mol% Cl at temperatures above T_g leads to the precipitation of silver nanoparticles with no shell (**Figure 5**). At the same time, such treatment of PTR glasses containing >1.0–2.2 mol% Cl results in the precipitation of silver nanoparticles with a shell consisting, according to Ref. [24], of mixed sodium and silver chlorides in a varied proportion (**Figures 4** and **5**). The evolution of absorption spectra during the photo-thermo-induced crystallization is shown in **Figure 4**. It can be seen that the heat treatment of nonirradiated chloride PTR glass has no measurable effect on the absorption spectra. According to calculations described in Ref.

[24], the sizes of silver nanoparticles and silver and sodium chloride nanocrystals are relatively small (about 3 nm [**Figure 7**] for silver nanoparticles, NPs, and 27 nm for nanocrystals). This is why chloride PTR glasses exhibit a rather low level of scattering.

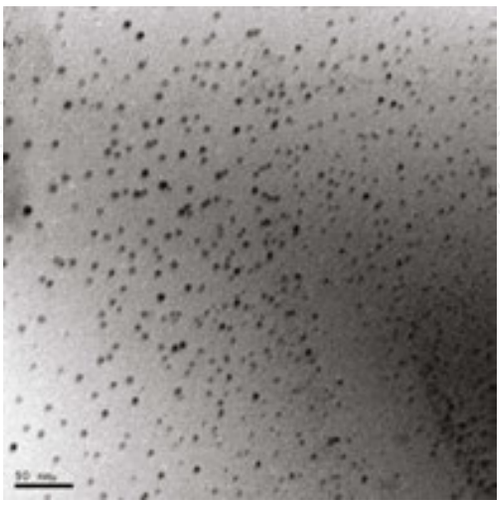


Figure 7. TEM image of silver nanoparticles in chloride PTR glass. Scale − 50 nm.

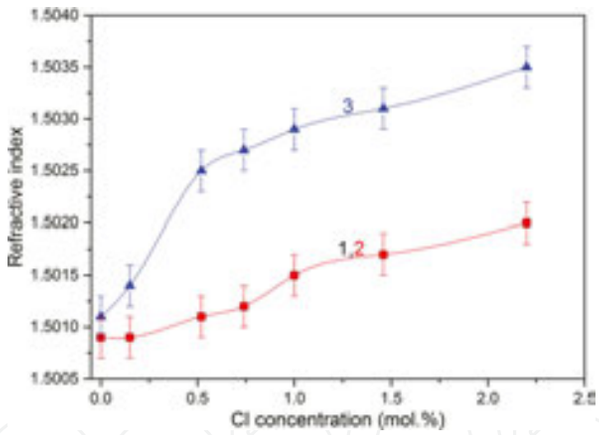


Figure 8. Effect of chlorine concentration on the refractive index (n_d) of PTR glass. 1—untreated glass samples, 2—glass samples after the heat treatment, 3—glass samples after the UV irradiation and subsequent heat treatment.

Figure 8 shows the evolution of the refractive index of PTR glass with an increase in the chlorine concentration for initial, heat-treated, and UV-irradiated and then heat-treated glasses (curves 1–3). As seen, the incorporation of Cl results in a consecutive increase in the refractive index of glass irrespective of treatment applied. In particular, Curves 1 and 2 coincide with each other, i.e., the heat treatment of nonirradiated chloride PTR glasses does not change their refractive index [24]. On the contrary, the UV irradiation and subsequent heat treatment of chloride PTR glasses result in a significant increase in their refractive index. For the maximum chlorine concentration, a difference Δn between the refractive index values of the UV-irradiated and nonirradiated glasses after the heat treatment reaches magnitudes up to 1.0×10^{-3}. The

positive increment of refractive index as well as high value of Δn in chloride PTR glasses can be used for recording VBGs and optical waveguides.

4. Properties of bromide PTR glasses

The bromide PTR glasses are photosensitive multicomponent glasses based on Na_2O-ZnO-Al_2O_3-SiO_2-NaF system doped with variable batch concentration of Br (0–1.5 mol%), photosensitizer, such as CeO_2 (0.01 mol%), reductant, such as Sb_2O_3 (0.05 mol%), and Ag_2O (0.1 mol %). The bromide PTR glass was designed and synthesized in ITMO University, Russia [17].

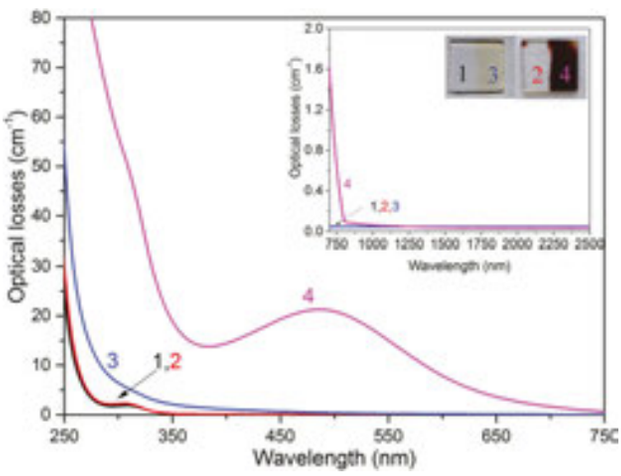


Figure 9. Absorption spectra of PTR glass containing 0.7 mol% Br (1) is the spectrum of initial untreated glass, (2) is the spectrum for glass after the UV irradiation for 50 s alone, (3) is the spectrum for glass after the heat treatment alone, and (4) is the spectrum for glass after the UV irradiation for 50 s and subsequent heat treatment. An inset shows the photos and absorption spectra (700–2500 nm) of treated bromide PTR glass samples containing 0.7 mol% Br. Here (1) is initial untreated glass, (2) is glass after the UV irradiation for 50 s alone, (3) is glass after the heat treatment alone, and (4) is glass after the UV irradiation for 50 s and subsequent heat treatment.

Initially, bromide PTR glasses are transparent in a wide range: 250–2500 nm (**Figure 9**). The substitution of chlorine by bromine in PTR glass composition affects the crystallization mechanism (**Figure 10**). The UV irradiation of bromide PTR glasses results in the Ce^{3+} ion photoionization and SMC formation (**Figure 9**); the latter playing the role of crystallization centers (**Figure 3(a)**). Heating all the studied bromide PTR glasses at temperatures above 250 C and less than T_g results, as shown in **Figure 3(b)**, in releasing electrons from Sb and capturing them by Ag ions with further formation of an extra amount of neutral silver atoms and molecular clusters [19]. The latter provides, according to Refs. [27, 29], a broadband luminescence in the visible and NIR ranges. Further, the heat treatment of PTR glasses containing 0.25–0.7 mol% Br at temperatures above T_g leads to the precipitation of silver nanoparticles with a silver bromide-based shell varying in thickness [20] and/or composition [30]; namely, mixed silver and sodium bromides can occur (**Figure 10(a)**). Moreover, the above heat treatment can result in shifting the plasmon resonance absorption band toward the greater wavelengths (**Figure 9**); such a treatment of PTR glasses containing from 1.0 to 1.5 mol% Br results in the

http://dx.doi.org/10.5772/66116

precipitation of small silver nanonoparticles without a perceptible plasmon resonance peak in the absorption spectrum (**Figure 11**)—the nanoparticles being covered by a shell consisting of silver bromide (**Figure 10(b)**). The sizes of silver nanoparticles and silver bromide nanocrystals are relatively small (<3 nm for silver NPs and <11 nm for nanocrystals).

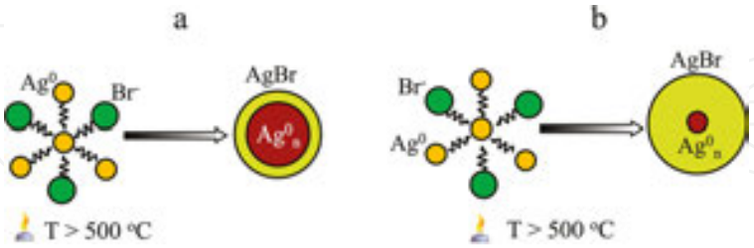


Figure 10. Scheme for the photo-thermo-induced crystallization mechanism inherent in bromide PTR glasses for various Br concentrations (0–1.5 mol%). (a) The photoactivation of PTR glass (Ce^{3+} ion photoionization), formation of neutral silver molecular clusters, and capturing electrons by Sb^{5+} valence states. (b) Releasing electrons by Sb and capturing them by Ag ions with the formation of neutral silver atoms and clusters, and (c) The growth of (i) silver nanoparticles with a shell composed of silver bromide in glasses containing 0.25–0.7 mol% Br or (ii) small silver nanoparticles characterized by broad plasmon resonance peak with a shell made of silver bromide nonocrystals in glasses containing 1–1.5 mol% Br.

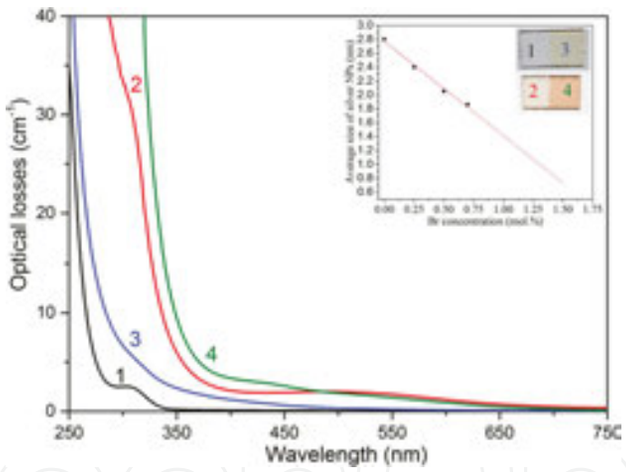


Figure 11. Absorption spectra of PTR glass containing 1 mol% Br (1) is the spectrum for initial untreated glass, (2) is the spectrum for glass after the heat treatment alone, (3) is that for glass after the UV irradiation for 50 s alone, and (4) is the one for glass after the UV irradiation for 50 s and subsequent heat treatment. An inset shows the effect of bromine concentration on the average size of silver nanoparticles (NP) calculated using Mie theory and the photos of bromide PTR glass containing 1 mol% Br at all stages of photo-thermo-induced crystallization (1) initial untreated glass, (2) glass after the heat treatment alone, (3) glass after the UV irradiation for 50 s alone and (4) is the one after the UV irradiation for 50 s and subsequent heat treatment.

Figure 12 shows the evolution of the PTR glass refractive index with an increase in the bromine concentration for initial, heat-treated, and UV-irradiated and then heat-treated glasses (curves 1–3). As is shown, the incorporation of Br leads to a consecutive increase in the refractive index of glass irrespective of treatment applied. In particular, curves 1 and 2 coincide with each other up to reaching the bromine concentration of 0.7 mol%. In other words, the heat treatment of

nonirradiated bromide PTR glasses with bromine concentration <1 mol% does not change their refractive index [13]. On the contrary, the UV irradiation and subsequent heat treatment of bromide PTR glasses result in a significant increase in their refractive index. For the maximum bromine concentration, a difference Δn between the refractive indices of the UV-irradiated and nonirradiated glasses after the heat treatment reaches magnitudes up to 0.8×10^{-3}.

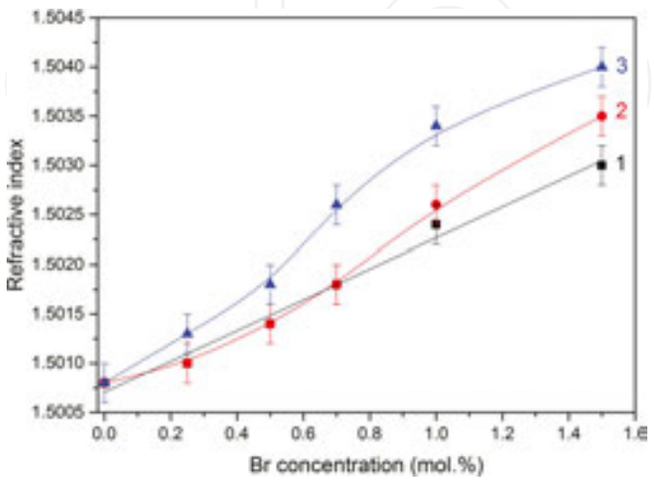


Figure 12. Effect of bromine concentration on the refractive index (n_d) of PTR glass. 1—untreated glass samples, 2—glass samples after the heat treatment, 3—glass samples after the UV irradiation and subsequent heat treatment.

5. Holographic properties of PTR glasses

Since the main purpose of the material is to serve as a holographic media, study of the refractive index dynamic range was held by utilizing holographic technique. For this purpose, Bragg gratings with period of 775 nm were recorded with UV radiation of He-Cd laser ($\lambda = 325$ nm). Conditions of thermal treatment as well as exposure schedule differed depending on glass type, due to the difference in the mechanism responsible for refractive index change. After UV exposure and thermal treatment, gratings were measured and analyzed using Collier [31] and Carretero [32] equations. All measurements were performed at the wavelength of He-Ne laser ($\lambda = 632.8$ nm). Analysis was made with respect to the form of the angular dependence contour either in the zero order or in the first-order of diffraction. Even though the gratings are quasi-sinusoidal, we confine our analysis and therefore material characterization with first harmonic of the refractive index modulation amplitude (RIMA). In this chapter, we will show the exposure dependencies of the RIMA for each glass and its behavior connected with thermal treatment schedule.

5.1. Fluoride PTR glass

In **Figure 13**, typical dependence of the RIMA on the UV exposure for our fluoride PTR glass is shown. One can see that there is a quite wide range of the exposures in which the RIMA is

http://dx.doi.org/10.5772/66116

at maximum. Therefore, we assume that an optimum exposure for this glass lies within 0.4–0.65 J/cm^2. Decreasing the RIMA with an increase in the exposure, we explain by the effect of the stray scattering of neutral silver clusters that appears during the recording process. This scattering affects the contrast of the interference pattern, thus lowering the RIMA in the grating.

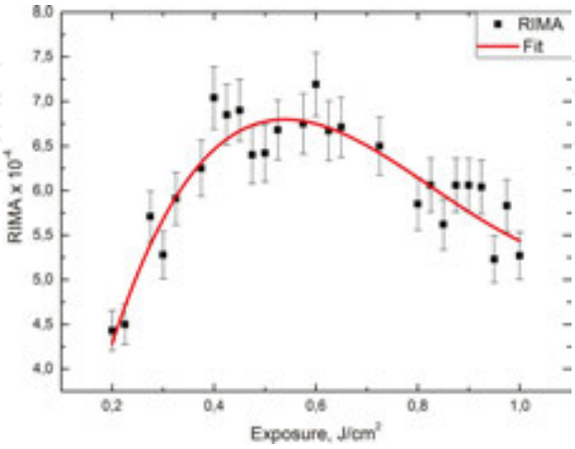


Figure 13. Dependence of the RIMA on exposure.

In **Figure 14**, the dependence of RIMA value on the duration of the thermal treatment is shown. One can see that this dependence is not linear. Basically, we can vary the duration together with temperature and obtain the same effect. For example, the RIMA value of 1.3×10^{-3} can be achieved for 8 h of thermal treatment at temperature of 500 C or for 130 h of heat treatment at temperature of 470°C.

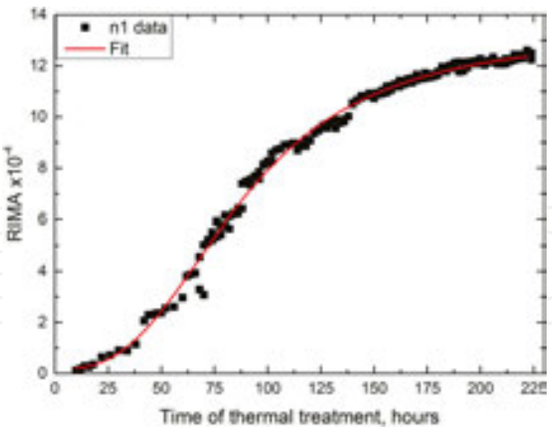


Figure 14. Refractive index modulation amplitude of the grating in the fluorine PTR glass with respect to duration of the thermal treatment.

Additional studies of glass chemical composition allowed for implementing the complex optimization of components, the main goal being to decrease optical losses in the visible spectral range caused by the absorption band of colloidal silver [12]. Components that had undergone the concentration optimization were as follows: halides (fluorides and bromides)

responsible for the growth of microcrystalline shell and crystalline phase; antimony that plays a key role in capturing and donating the photoelectrons arising upon the irradiation of cerium and subsequent thermal treatment of PTR glass; also, the concentration of impurities capable of capturing photoelectrons was lowered. As a result, a number of parameters were improved, thus exceeding those of commercially produced material. First of all, the problem of undesirable absorption in the visible spectral range was solved, which resulted in a great decrease in the induced optical losses caused by colloidal silver. PTR glass with the renewed composition shows, after the FTI crystallization process, no absorption band related to the colloidal particles in the optical loss spectra of a sample with a hologram recorded (**Figure 15**).

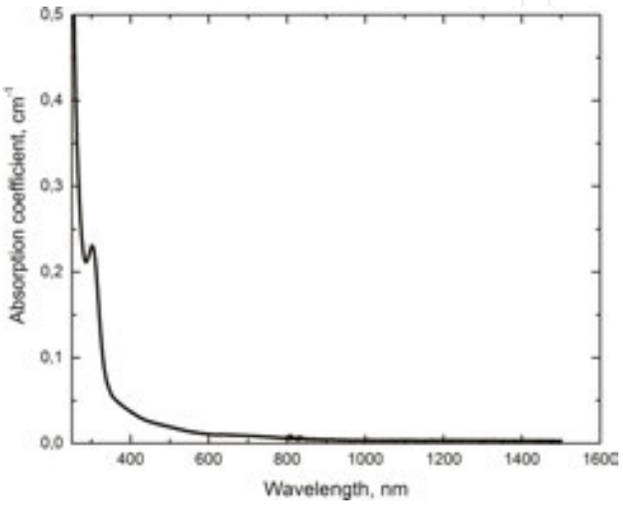


Figure 15. Absorption coefficient spectra of modified PTR glass with a hologram recorded.

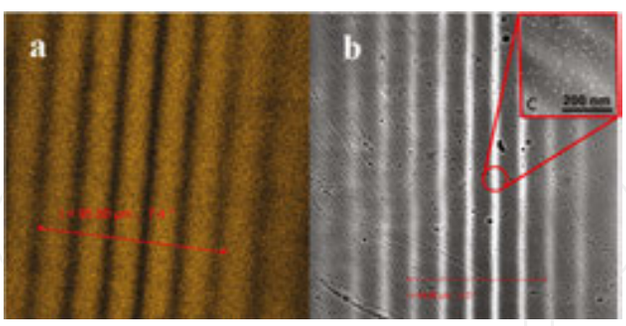


Figure 16. Microscope image of the grating (a) right after the UV exposure and (b) after the heat treatment, and TEM image of the grating fringe (c).

Nowadays, the maximum RIMA for the fluoride PTR glass can be as high as 1.5×10^{-3}. If we neglect scattering by the crystalline phase inside the glass, the maximum RIMA magnitude can be even greater (like 2.5×10^{-3}).

Also, we performed the visualization of the recorded gratings right after an exposure with the UV radiation (**Figure 16(a)**) and after the heat treatment (**Figure 16(b)**). In **Figure 16(a)**, one

http://dx.doi.org/10.5772/66116

can see the luminescence of the silver clusters in accord with the interference pattern, whereas, in **Figure 16(b)**, there is the grating itself only formed with NaF crystals.

5.2. Chloride PTR glass

We only started studying the holographic characteristics of this type of PTR glasses. By now, investigations carried out were intended, by analogy with similar studies performed earlier for fluoride glasses, to estimate the maximum possible changes in the RIMA for these glasses.

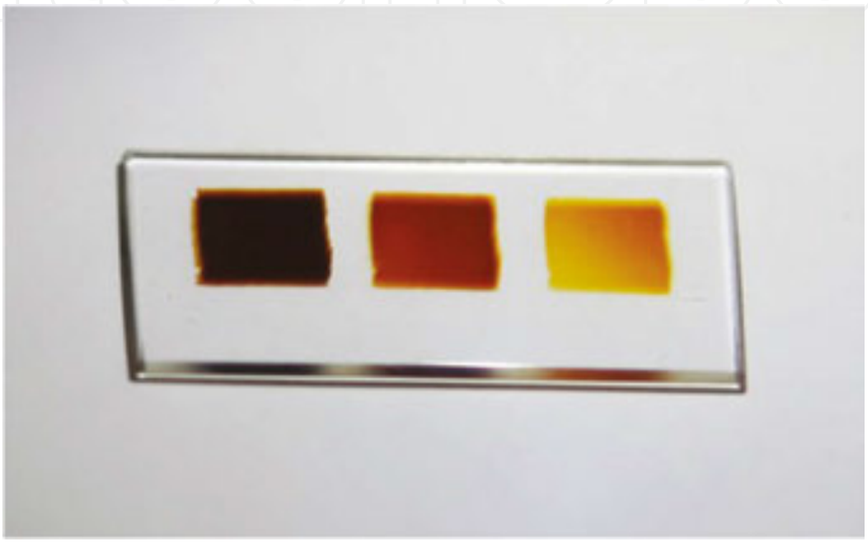


Figure 17. Image of the sample with gratings recorded.

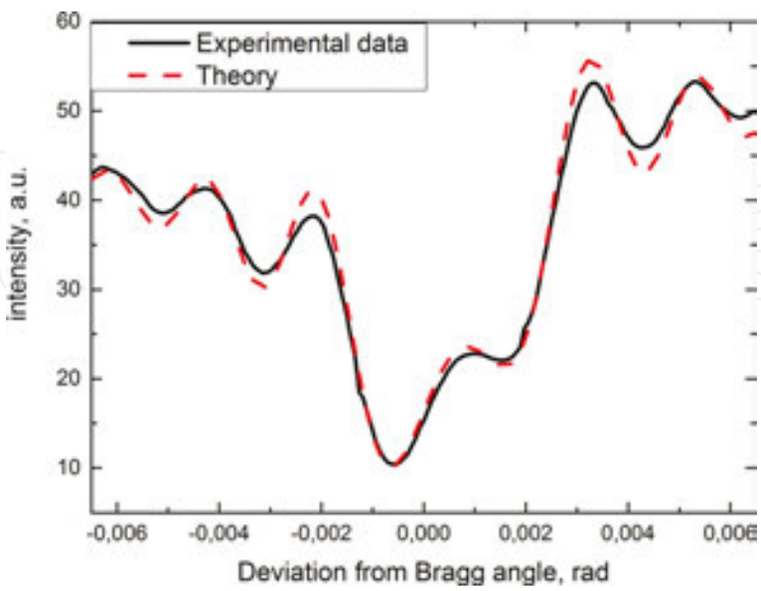


Figure 18. Example of the angular response of the mixed absorption—the phase holographic grating recorded in chloride PTR glass.

Gratings recoded on this glass are colored (**Figure 17**), which is why it is natural to assume the modulation of absorption in the grating. The first measurements performed on these gratings proved the validity of this assumption. As one can see in **Figure 18**, the angular response from the grating, indeed, has a poor symmetry. So far measurements were only at a single wavelength of 632.8 nm that is far enough from the resonance band of silver nanoparticles. Hence, the value of the absorption index modulation amplitude (AIMA) was expected to be rather small.

Figure 18 shows the approximation of experimentally obtained angular response in zero order with a theoretical curve. The position of the central maximum of the latter is shifted, and the positions of side lobes are perfectly fitted to the experimental curve. Differences in the intensities of the side lobes are connected with scattering in the sample that is inflicted by silver nanoparticles. It is also clear that this grating has a strong RIMA because the shape of the contour includes a lot of side lobes and actually lacks the central maximum.

On the other hand, our theoretical analysis shows that the AIMA is quite weak compared with other materials. The reason can be due to the fact that the measurements are conducted in a region lying far enough from the main resonance band of the silver nanoparticles. For instance, AIMA for a sample subjected to the thermal treatment for 30 h and exposure of 4 J/cm^2 is found to be almost 6 cm^{-1}, which consists 85% of the total value of the absorption coefficient at this wavelength (7.12 cm^{-1}). The fact that AIMA is a bit less than the latter can be explained in two ways. First, the occurrence of scattering during the recording process might create clusters outside the interference pattern, hence, lowering the contrast. Second, as seen in figure below, glass is colored even outside the irradiated region (pale red color); this can be also the reason for an additional increase in the absorption coefficient that is not connected with AIMA.

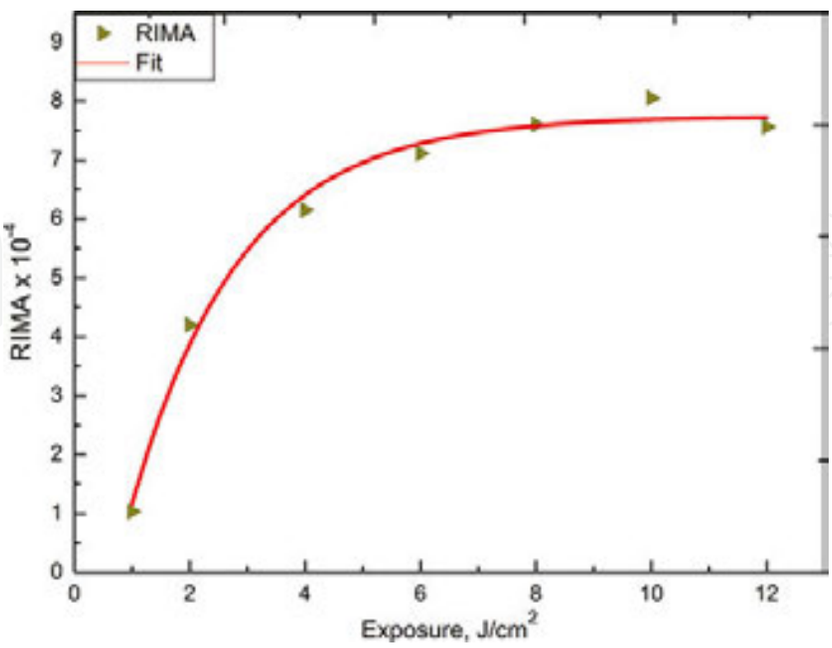


Figure 19. Typical dependence of the RIMA on exposure for chloride PTR glass.

http://dx.doi.org/10.5772/66116

According to this fact, one can expect the total absorption coefficient to be modulated in the region of resonance band, which can lead to really great AIMA magnitudes. In **Figure 19**, a typical dependence of the RIMA on exposure is shown.

As is seen, this type of glass demonstrates some kind of saturation. One can conclude that, after a dose of 4–6 J/cm^2, changes in the RIMA do not depend on exposure and are only affected by heat treatment. Our studies show that this kind of glass can acquire almost the same change in the refractive index as fluoride ones. The maximum value of RIMA was found to be ~11×10^{-4}.

This type of glass allows for recording the mixed amplitude-phase gratings alone, and it is hard to find an application for such gratings. But since it was shown that AIMA is much smaller than it was expected to be, and on the other hand, RIMA is as strong as in fluoride glass, one can make quite a promising suggestion that bleaching of this glass would not affect the RIMA component of the grating. Therefore, we can utilize positive refraction index change with its rather big value of 1×10^{-3}.

5.3. Bromide PTR glass

As mentioned above, bromine PTR glass is characterized by mechanism of induced refractive index variation nearly in the same manner as that for chloride glasses. Now, bromine PTR glass remains to be a novel material that is not well investigated yet. Data available by now indicate this kind of glass to have very low refractive index change compared with that, for example, of chloride PTR glasses. A preliminary investigation of holographic properties of this material shows that, if we record a grating on the latter, the RIMA magnitudes are quite low and do not exceed 1×10^{-4}. Like the spectra of chloride glasses, those of bromide ones have the absorption band in the visible region, which means that holograms recorded on this glass are mixed, i.e., have both RIMA and AIMA. Up to now, it remains unclear what is the reason for such a low contrast of the refractive index in the gratings, although the absolute refractive index variation was shown to be at least as high as 8×10^{-4}. There can be several possible reasons responsible for this effect. One of the reasons can be the high scattering in the material during the recording process that leads to a decrease in the contrast of the interference pattern inside the medium. Second possible reason can be the mobility of the clusters inside the medium during the process of heat treatment. We have already demonstrated this effect for chloride PTR glasses in which the nonirradiated areas had slightly colored regions around the gratings. This area has a color the same as that of the gratings themselves, which is why we can assume that silver nanoparticles have a shell structure the same as that inside the irradiated area; hence, a decrease in the contrast. It is unclear, however, why these effects are weaker in chloride glass, thus allowing for gaining the much greater contrast of the refractive index compared with that attainable with bromide glasses.

A typical dependence of the RIMA for bromide PTR glass is shown in **Figure 20**. As seen, the dependence reveals some kind of saturation and reaches its maximum around 4 J/cm^2 with no further changes. This pattern is similar to that observed for chloride glass and differs from that observed for fluoride glass. This can be taken as a proof that the mechanisms responsible for the refractive index modulation in the bulk of these two glass types are similar. In summary, we can state that, so far, the RIMA in the gratings on the bromide PTR glass is rather low and

does not exceed 1×10^{-4}, though this value differs from that obtained with absolute measurements, ~8×10^{-4}.

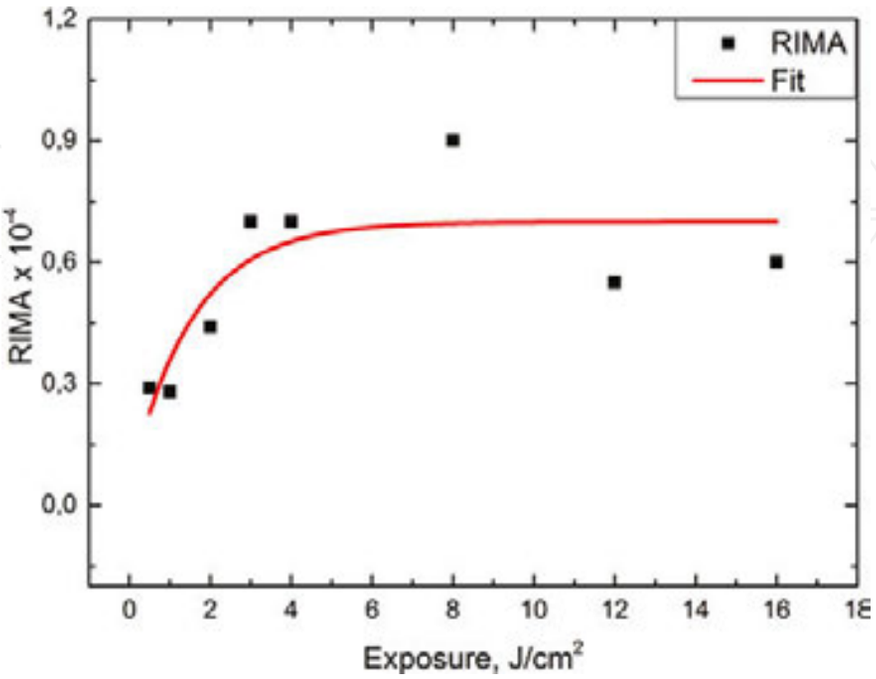


Figure 20. Typical dependence of the RIMA on exposure for bromide PTR glass.

6. Holographic optical elements

PTR glass is a bulk material that is characterized by high homogeneity. Therefore, it is possible to manufacture gratings with high efficient thickness (say, about 1 mm and more). The use of high thickness of the material opens up a possibility to manufacture spatial and spectral filters with outstanding parameters. As known, the selectivity of the Bragg grating depends on its thickness; therefore, it is possible to create gratings with sub nm spectral selectivity and with angular selectivity of <1 angular min.

6.1. Super narrow-band filters for laser diodes and their temperature stabilization of radiation

The widespread use of semiconductor lasers is stimulated by a number of their advantages [33–35] such as the high efficiency (75–80%), small sizes, simplicity of operation, and relatively low cost. An important advantage of semiconductor lasers is also the possibility of fabricating emitters operating at different wavelengths in the visible, near-infrared, and mid-infrared spectral ranges. Apart from the above beneficial features, the semiconductor lasers have certain drawbacks: their emission is quasi-monochromatic and spectrally unstable. This is caused by a number of factors. The broadening of the lasing spectrum under an increase in the injection

http://dx.doi.org/10.5772/66116

current stems from the fundamental aspects of charge-carrier transport and captures into the quantum-confined active region. The lasing spectrum is also affected by the multimode design of the laser cavity. A shift of the spectrum occurs as a result of heating the active region with an increase in the injection current, which causes a reduction in the band gap and, thus, the shift of the lasing spectrum to the longer wavelengths.

This problem can be solved by means of VBG recorded in photo-thermo-refractive glass. Due to high spectral selectivity of recorded holograms, the implementation of such grating inside the external cavity of laser diode can significantly narrow the output spectra. This idea was used widely and proved its advantages. External cavity design based on the VBG can vary (see **Figure 21**), as well as both reflecting or transmitting Bragg grating can be used [26].

The simplest implementation of VBG as an external cavity element is shown in **Figure 21(a)**, where a radiation after being passed through the collimating lens falls normally on the VBG element. Unfortunately, due to a high divergence along the fast axis of the LD output radiation, it is impossible to create the reliable external cavity of LD without additional collimation optics. **Figure 21(b)** shows typical design of external cavity using transmission Bragg grating. The grating works backward and forward, and its diffraction efficiency has to be lower than 80% to couple output radiation efficiently. So there is a need for an additional mirror in the cavity setup to reduce the power loss through the nondiffracted radiation on backward cavity trip. The position of mirrors can be changed, but the number of output channels will remain the same. Also, the cavity designs for coupling the higher-order modes of the LD are also possible. Such designs require the high diffraction efficiency of the grating to provide the maximum output performance and are suitable for wide stripe emitting diodes. Stabilized by means of VBG, the laser diodes show a stable output in the temperature range from 15°C to 75°C [36].

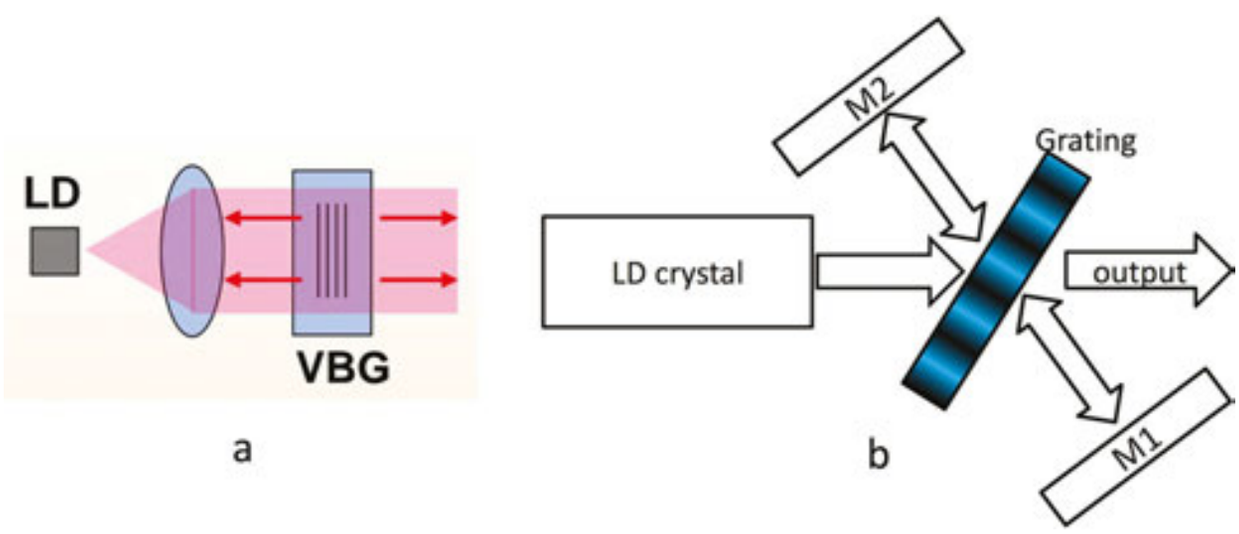


Figure 21. Examples of design of external cavity of a diode laser based on VBGs (a) is an example of reflecting VBG implementation and (b) is an example of cavity based on transmitting VBG.

Recent studies of VBG-based external cavity LD show that the implementation of the grating inside cavity significantly increases its selective properties. For example, a grating used in our

experiment [37] was recorded with estimated spectral selectivity as great as ~2 nm. We used a cavity shown in **Figure 21(b)** with the transmitting VBG. The emission spectra from such cavity show us two longitudinal modes with the separation of 100 pm and bandwidth of 4–8 pm (**Figure 22**).

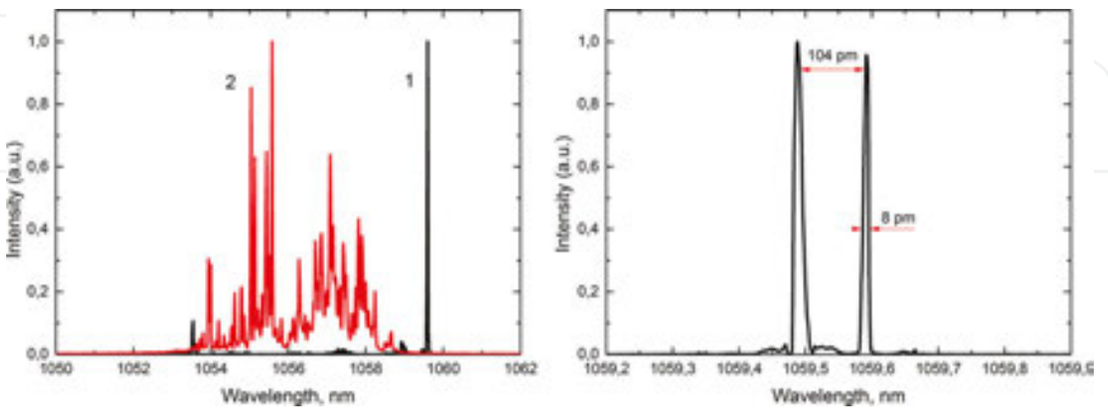


Figure 22. Emission spectra of laser diode source. Left: spectra recorded with (1) and without (2) grating. Right: the detailed view of the emission line [36].

Similar to the conventional ways of LD stabilization such as Littrow scheme and Litman-Metcalf configurations, using the standard diffraction gratings based on the VBG in the external cavities can provide tuning of the output emission of the source. Merely by the rotation of the grating, we can achieve a tunability along all the gain spectra of the semiconductor crystal that can be really huge, up to 60 nm. An example of such tuning is shown in **Figure 23**.

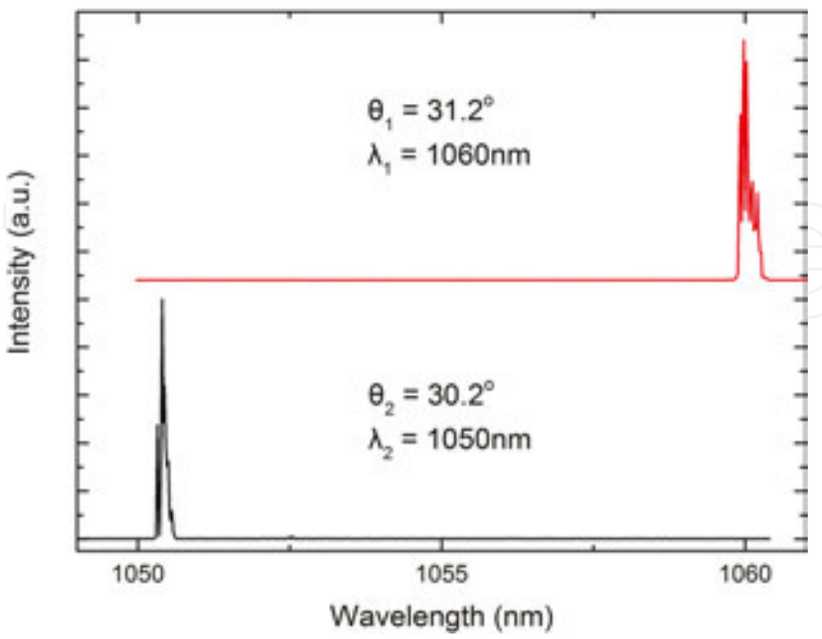


Figure 23. Emission spectra of the external cavity laser diode with different angles of VBG.

http://dx.doi.org/10.5772/66116

6.2. Laser beam combiners

The diffraction efficiency directly depends on the thickness and RIMA, and as shown, this glass has quite a big inflicted refractive index change. Therefore, it is also possible to record multiple gratings inside the single volume of the glass (**Figure 24**).

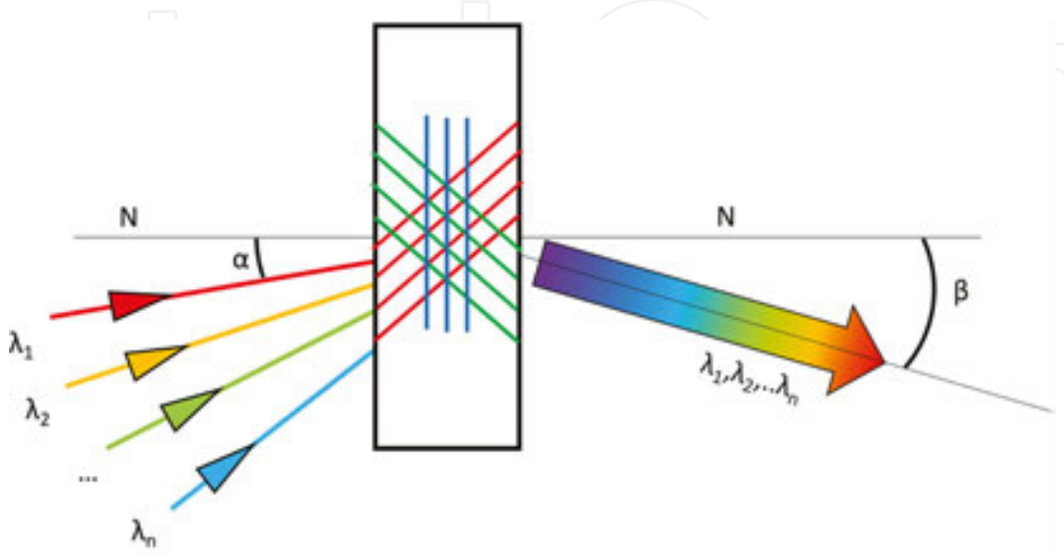


Figure 24. Example of multiple gratings recorded in the single volume of the glass for spectral beam combining.

There is much interest in the use of spectral beam combining (SBC) to combine multiple high-power laser beams into a single high-power one with a narrow spectral linewidth and good beam quality [38]. This idea can be implemented by using several volumes of Bragg gratings for each channel multiplexed in the single volume of PTR glass. Recently, a two and four channel combiner based on the multiplexed reflective Bragg gratings was reported [39]. This approach allows one to develop a combining system with low complexity and better robustness.

6.3. Collimator sights

The holographic collimator sights are the development of the classical collimator sights. This new kind of design provides the greater transparency of the working aperture compared with the classical collimator and greater parallax suppression. This kind of sights has an open design, which means that the sight can be aimed with both eyes. So a shooter can use the peripheral vision and engage more effectively. Also, due to the properties of a hologram, such sight is very resistant to various injuries and pollution. The hologram is recorded over the entire area of the aperture, which is why the sight remains in the working condition even after a partial pollution and/or damage. Also, one of the main advantages over the conventional sights is the absence of a flare toward a target, which is crucial in a combat.

Basic elements of a holographic sight are shown in **Figure 25**. The operation principle of holographic collimator sights can be briefly described as follows. A radiation from the light

source falls on the recorded hologram that creates an image of the recorded mark in the image plane. The high transparency of PTR glass in the visible range (above 90% without AR coating) opens up this field of applications.

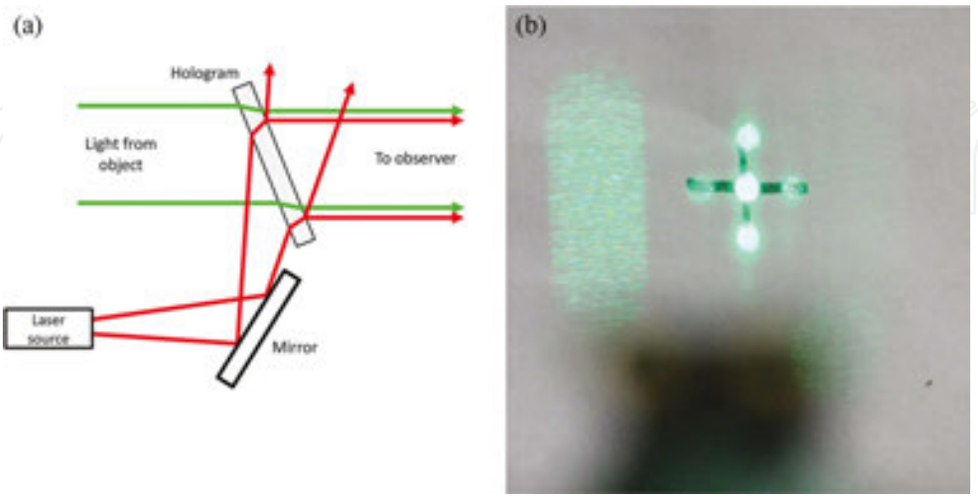


Figure 25. Holographic sight (a) is the basic scheme of the sight and (b) is the observable image of a mark recorded on PTR glass.

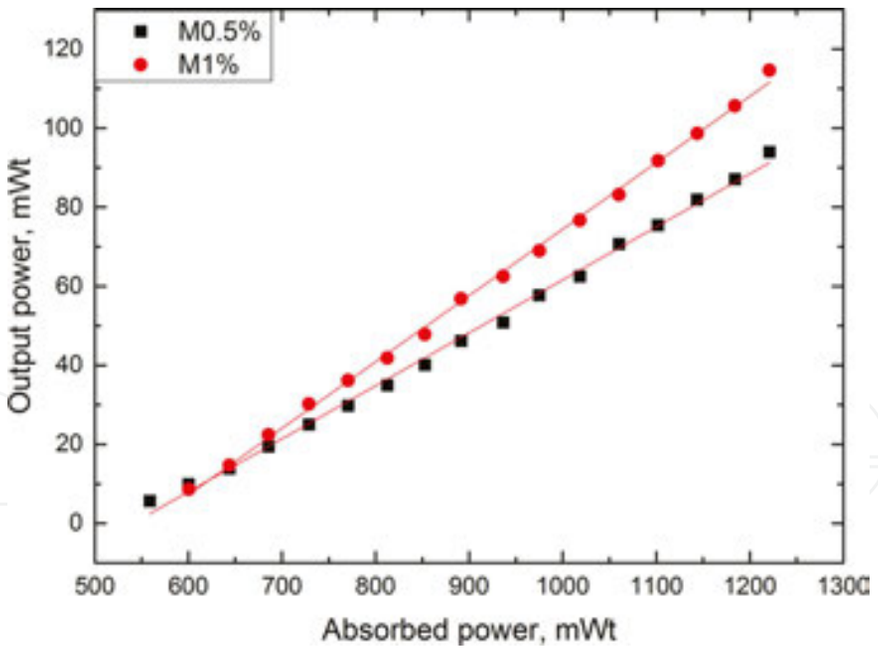


Figure 26. Laser action of Nd^{3+} heavily doped ($N_{Nd} = 2.5 \times 10^{20}$) PTR glass measured for mirrors with the reflection of 1% (red curve) and 5% (black curve) [34].

The application of PTR glass can solve the problem of image stabilization, which is necessary due to the instability of laser diode source used in such sights. To date, this problem is solved by adding, into the optical scheme, the achromatizing diffraction elements such as thin

gratings, complex two-cavity mirrors, or compound objectives. The wavelength shift caused by laser diode temperature changes can be nullified by spectral selectivity of thick hologram recorded on PTR glass. Because the diffraction efficiency of holograms on PTR glass can reach values of ~95%, an intensity required for the mark observation is rather low. In **Figure 25**, the observable image of holographic mark recorded on PTR glass is demonstrated.

6.4. Distributed feedback (DFB) and distributed Bragg reflector (DBR) lasers

The concept of DFB lasers was originally demonstrated in 1971 [40] when the laser output from a gelatin film on a glass substrate was obtained for the first time. Two years later [41], a generation from a similar structure on GaAs at nitrogen temperatures was demonstrated. Benefits of such a laser design are pretty obvious: Bragg grating acts as a selective mirror with very narrow reflection bandwidth and, thus, provides a narrow spectral emission output. Since then, DFB lasers had a lot of development, but yet there were no results in creating DFB solid-state lasers.

Doping PTR glass with rare earth elements provides an access to the construction of DFB and DBR lasers because such medium possesses both the laser and holography properties. Recently, first results on laser action on PTR glass were obtained [42, 43]. Later, a generation on heavily Nd-doped PTR glass was obtained in ITMO University [44]. Laser performance is shown in **Figure 26**. Our calculation shows that PTR glass itself is characterized, due to its outstanding homogeneity, by relatively low round trip loss estimated to be ~0.26%, which is comparable to that of commercially fabricated Nd:YAG crystals.

Further investigations of DFB/DBR effect on PTR glass showed that recording a grating inside PTR glass does not affect its lasing properties. For instance, the laser action in the DFB/DBR configuration on Nd- and Yb-doped PTR glasses was demonstrated [45]. In these experiments, the output radiation from both setups (DFB/DBR) and on both types of PTR glasses (Nd and Yb) was obtained. The emission spectra observed show a narrow line with 30 pm bandwidth.

7. Conclusions

Recent achievements of ITMO University (St. Petersburg, Russia) in developing new holographic media such as fluoride, chloride, and bromide photo-thermo-refractive (PTR) glasses are demonstrated. PTR glasses change their refractive index after an exposure to the near-UV radiation followed by thermal treatment at temperatures close to the glass transition one. In the case of fluoride PTR glass, the increment of the refractive index is negative and its magnitude reaches 1.5×10^{-3} ppm. In the case of chloride and bromide PTR glasses, the increment of the refractive index is positive and its magnitudes reach 1.0×10^{-3} and 0.8×10^{-3} ppm, respectively. Thus, the fluoride, chloride, and bromide PTR glasses are very promising photosensitive materials for recording the 3D-phase holographic optical elements. Some examples of holographic optical elements based on PTR glasses are demonstrated such as the supernarrow-band spectral filter for laser diodes, laser beam combiners, the holographic marker for the collimating sight, and lasers with Bragg and distributed feedback.

Acknowledgements

Research was funded by Russian Science Foundation (Agreement #14-23-00136)

Author details

Nikonorov Nikolay, Ivanov Sergey*, Dubrovin Victor and Ignatiev Alexander

*Address all correspondence to: ykkapoh@gmail.com

Saint-Petersburg National Research University of Information Technologies, Mechanics and Optics, St. Petersburg, The Russian Federation

References

[1] Stookey SD, Beall GH, Pierson JE. Full-color photosensitive glass. *J Appl Phys*. 1978;49(10):5114. DOI:10.1063/1.324458.

[2] Pierson JE, Stookey SD. United States Patent 4,057,408. 1977.

[3] Pierson EJ, Stookey SD. United States Patent 4,017,318. 1977.

[4] Panysheva EI, Tunimanova IV, Tsekhomskiĭ VA. A Study of Coloring in Polychromatic Glasses. *Fiz Khim Stekla*. 16(2):239–244 (In Russian).

[5] Dotsenko AV, Efimov AM, Zakharov VK, Panysheva EI, Tunimanova IV. On the absorption spectra of polychromatic. *Fiz Khim Stekla*. 1985;11(5):592–595 (in Russian).

[6] Glebov LB, Nikonorov NV, Panysheva EI, et al. New possibilities of photosensitive glasses for the recording of volume phase diagrams. *Opt Spektros*. 1992;73(2):404–412 (in Russian).

[7] Kuchinskii SA, Nikonorov NV, Panysheva EI, Savvin VV, Tunimanova IV. Properties of volume phase holograms on polychromatic glasses. *Opt Spektrosk*. 1991;70(6):1286–1300 (in Russian).

[8] Nikonorov N.V., Panysheva E.I., Savvin V.V., and Tunimanova I.V., Polychromatic Glasses-A New Medium for Optical Data Recording, "Opticheskoe izobrazhenie i registriruyushchie sredy" (Proceedings of All-Union Conference "Optical Image and Recording Media"), Leningrad, Russia, 1990, 2 p. 48.

[9] Glebov LB, Nikonorov NV, Panysheva EI, Tunimanova IV, Savvin VV, Tsekhomskii VA. Photothermorefractive glass. In: IF AN Latv. SSR, ed. *Trudy VII Vsesoyuznoi Konferentsii Po Radiatsionnoi Fizike I Khimii Neorganicheskikh Materialov (Proceedings of VII All-Union*

Conference on Radiation Physics and Chemistry of Inorganic Materials). Riga; 1989:527 (in Russian).

[10] Efimov OM, Glebov LB, Glebova LN, Richardson KC, Smirnov VI. High efficiency Bragg gratings in photo-thermo-refractive glass. *Appl Opt*. 1999;38(2):619–627.

[11] Glebov LB, Glebova LN, Richardson KA, Smirnov VI. Photo-induced processes in photo-thermo-refractive glasses. In: Soc AC, ed. *Proceedings of XV Congress on Glass*. San Francisco; 1998.

[12] Ivanov SA, Ignat AI, Nikonorov NV, Aseev VA. Holographic characteristics of a modified photothermorefractive glass. *J Opt Technol*. 2014;81(6):356–360. DOI:10.1364/JOT.81.000356.

[13] Nikonorov NV, Panysheva EI, Tunimanova IV, Chukharev AV. Influence of glass composition on the refractive index change upon photothermoinduced crystallization. *Glas Phys Chem*. 2001;27(3):241–249. DOI:10.1023/A:1011392301107.

[14] Glebova L, Lumeau J, Klimov M, Zanotto ED, Glebov LB. Role of bromine on the thermal and optical properties of photo-thermo-refractive glass. *J Non-Cryst Solids*. 2008;354(2–9):456–461. DOI:10.1016/j.jnoncrysol.2007.06.086.

[15] Glebov LB, Nikonorov NV, Panysheva EI, et al. New ways to use photosensitive glasses for recording volume phase holograms. *Opt Spectrosc*. 1992;73(2):237–241.

[16] Dyamant I, Abyzov AS, Fokin VM, et al. Crystal nucleation and growth kinetics of NaF in photo-thermo-refractive glass. *J Non-Cryst Solids*. 2013;378:115–120. DOI:10.1016/j.jnoncrysol.2013.06.027.

[17] Nikonorov N, Aseev V, Ignatiev A, Kolobkova E. SA. Novel glasses and nanoglasscer-amics for photonic and plasmonic applications. In: *Thirteenth International Conference onthe Physics of Non-Crystalline Solids*; 16–20 September 2012; Yichang Three Gorges, China; 201,. p. 89

[18] Cardinal T, Efimov OM, Francois-Saint-Cyr HG, Glebov LB, Glebova LN, Smirnov VI. Comparative study of photo-induced variations of X-ray diffraction and refractive index in photo-thermo-refractive glass. *J Non-Cryst Solids*. 2003;325(1–3):275–281. DOI: 10.1016/S0022-3093(03)00310-7.

[19] Mock JJ, Smith DR, Schultz S. Local refractive index dependence of plasmon resonance spectra from individual Nanoparticles. *Nano Lett*. 2003;3(5):485–491. DOI:10.1021/nl0340475.

[20] Nikonorov NV, Sidorov AI, Tsekhomskiĭ VA, Lazareva KE. Effect of a dielectric shell of a silver nanoparticle on the spectral position of the plasmon resonance of the nanoparticle in photochromic glass. *Opt Spectrosc*. 2009;107(5):705–707. DOI:10.1134/S0030400X09110058.

[21] Lumeau J, Glebova L, Golubkov V, Zanotto ED, Glebov LB. Origin of crystallization-induced refractive index changes in photo-thermo-refractive glass. *Opt Mater (Amst)*. 2009;32(1):139–146. DOI:10.1016/j.optmat.2009.07.007.

[22] Efimov AM, Ignatiev AI, Nikonorov NV, Postnikov ES. Quantitative UV–VIS spectroscopic studies of photo-thermo-refractive glasses. I. Intrinsic, bromine-related, and impurity-related UV absorption in photo-thermo-refractive glass matrices. *J Non-Cryst Solids*. 2011;357(19–20):3500–3512. DOI:10.1016/j.jnoncrysol.2011.06.031.

[23] Nikonorov N, Dubrovin V, Ignatiev A, Nuryev R, Sidorov A. Effect of halogens on phase separation, spectral and luminescent properties of photothermorefractive glasses. In: *12th International Conference on the Structure of Non Crystalline Materials, Programe and Abstracts*; 7 – 12 Jule 2013; Trento, Italy; 2012, p. 51.

[24] Dubrovin VD, Ignatiev AI, Nikonorov NV. Chloride photo-thermo-refractive glasses. *Opt Mater Express*. 2016;6(5):1701. DOI:10.1364/OME.6.001701.

[25] Sgibnev YM, Nikonorov NV, Vasilev VN, Ignatiev AI. Optical gradient waveguides in photo-thermo-refractive glass formed by ion exchange method. *J. Lightw. Technol.* 2015;33(17):3730–3735.

[26] Nikonorov N, Aseev V, Ignatiev A, Zlatov A. New polyfunctional photo-thermo-refractive glasses for photonics applications. In: Technical Digest of *7th International Conference on Optics-Photonics Design & Fabrication*; 19 – 21 April 2010; Yokohama, Japan; 2010, p. 209–210.

[27] Dubrovin VD, Ignatiev AI, Nikonorov NV, Sidorov AI, Shakhverdov TA, Agafonova DS. Luminescence of silver molecular clusters in photo-thermo-refractive glasses. *Opt Mater (Amst)*. 2014;36(4):753–759. DOI:10.1016/j.optmat.2013.11.018.

[28] Dubrovin VD, Ignat'ev AI, Nikonorov NV, Sidorov AI. Influence of halogenides on luminescence from silver molecular clusters in photothermorefractive glasses. *Tech Phys*. 2014;59(5):733–735. DOI:10.1134/S1063784214050107.

[29] Sgibnev YM, Nikonorov NV, Ignatiev AI. Luminescence of silver clusters in ion exchanged cerium-doped photo-thermo-refractive glasses. J Lumin. 2016;176:292–297. DOI:10.1016/j.jlumin.2016.04.001.

[30] Sinistri C, Riccardu R, Margheritis C, Tittarelli P. Thermodynamic Properties of Solid Systems AgCl + NaCl and AgBr + NaBr from Miscibility Gap Measurements. *Zeitschrift für Naturforsch A*. 1972;21(1):149–154.

[31] Collier R. J., Burckhardt C. B., Lin L. H. in Academic press New York and London. Optical holography Ch. 9; 1971. p. 277–279 DOI:10.1016/B978-0-12-181050-4.50021-4.

[32] Carretero L, Madrigal RF, Fimia a, Blaya S, Beléndez a. Study of angular responses of mixed amplitude—phase holographic gratings: shifted Borrmann effect. *Opt Lett*. 2001;26(11):786–788. http://www.ncbi.nlm.nih.gov/pubmed/18040450.

[33] Hofmann P, Amezcua-correa R, Antonio-lopez E, et al. Strong Bragg gratings in highly photosensitive photo-thermo-refractive-glass optical fiber. *IEEE Photonics Technol Lett*. 2013;25(1):25–28. DOI:10.1109/LPT.2012.2227308.

[34] Crump P, Erbert G, Wenzel H, et al. Efficient high-power laser diodes. IEEE J Sel Top Quantum Electron. 2013;19(4):1501211–150121. DOI:10.1109/JSTQE.2013.2239961.

[35] Tarasov IS. High-power semiconductor separate-confinement double heterostructure lasers. *Quantum Electron*. 2010;40(8):661–681. DOI:10.1070/QE2010v040n08ABEH014375.

[36] Pikhtin NA, Slipchenko SO, Sokolova ZN, et al. 16 W continuous-wave output power from 100 μm-aperture laser with quantum well asymmetric heterostructure. *Electron Lett*. 2004;40(22):1413–1414. DOI:10.1049/el:20045885.

[37] Venus GB, Sevian A, Smirnov VI, Glebov LB. High-brightness narrow-line laser diode source with volume Bragg-grating feedback. *Proc SPIE*. 2005;5711:166–176. DOI: 10.1117/12.590425.

[38] Fan TY, Member S. Laser beam combining for high-power. *High-Radiance Sources*. 2005;11(3):567–577. DOI:10.1109/JSTQE.2005.850241.

[39] Ott D, Divliansky I, Anderson B, Venus G, Glebov L. Scaling the spectral beam combining channels in a multiplexed volume Bragg grating. Opt. Express 2013;21(24): 29620–29627. DOI:10.1364/OE.21.029620.

[40] Kogelnik H, Shank CV. Stimulated emission in a periodic structure. *Appl Phys Lett*. 1971;18(4):152–154. DOI:10.1063/1.1653605.

[41] Nakamura M, Yen HW, Yariv A, Garmire E, Somekh S, Garvin HL. Laser oscillation in epitaxial GaAs waveguides with corrugation feedback. *Appl Phys Lett*. 1973;23(5):224–225. DOI:10.1063/1.1654867.

[42] Sato Y, Taira T, Smirnov V, Glebova L, Glebov L. Continuous-wave diode-pumped laser action of Nd^{3+}-doped photo-thermo-refractive glass. *Opt Lett*. 2011;36(12):2257–2259. DOI:10.1364/OL.36.002257.

[43] Ivanov SA, Ignatiev AI, Nikonorov NV. Advances in photo-thermo-refractive glass composition modifications. *Proc SPIE*. 2015;9508:95080E. DOI:10.1117/12.2178651.

[44] Ivanov SA, Lebedev VF, Ignat'ev AI, Nikonorov NV. Laser action on neodymium heavily doped photo-thermo-refractive glass. In Proccedengs of 1st International Symposium on Advanced Photonic Materials; 27 June – 1 July 2016; Saint Petersburg, Russia; p. 29–31.

[45] Ryasnyanskiy A, Vorobiev N, Smirnov V, et al. DBR and DFB lasers in neodymium- and ytterbium-doped photothermorefractive glasses. *Opt Lett*. 2014;39(7):2156–2159. DOI:10.1364/OL.39.002156.

IntechOpen

IntechOpen